

Competition between magnetic order and charge localization in Na_2IrO_3 thin crystal devices

Josue Rodriguez,¹ Gilbert Lopez,² Samantha Crouch,¹ Nicholas P. Breznay,³ Robert Kealhofer,² Vikram Nagarajan,² Drew Latzke,² Francisco Ramirez,¹ Naomy Marrufo,¹ Peter Santiago,⁴ Jared Lara,¹ Amirari Diego,¹ Everardo Molina,¹ David Rosser,¹ Hadi Tavassol,⁴ Alessandra Lanzara,² James G. Analytis,² and Claudia Ojeda-Aristizabal¹

¹⁾*Department of Physics and Astronomy, California State University Long Beach, Long Beach, California 90840, USA*

²⁾*Department of Physics, University of California Berkeley, California 94720, USA*

³⁾*Department of Physics, Harvey Mudd College, Claremont, California 91711, USA*

⁴⁾*Department of Chemistry and Biochemistry, California State University Long Beach, Long Beach, California 90840, USA*

(Dated: 13 February 2020)

Spin orbit assisted Mott insulators such as sodium iridate (Na_2IrO_3) have been an important subject of study in the recent years. In these materials, the interplay of electronic correlations, spin-orbit coupling, crystal field effects and a honeycomb arrangement of ions bring exciting ground states, predicted in the frame of the Kitaev model. The insulating character of Na_2IrO_3 has hampered its integration to an electronic device, desirable for applications, such as the manipulation of quasiparticles interesting for topological quantum computing. Here we show through electronic transport measurements supported by Angle Resolved Photoemission Spectroscopy (ARPES) experiments, that electronic transport in Na_2IrO_3 is ruled by variable range hopping and it is strongly dependent on the magnetic ordering transition known for bulk Na_2IrO_3 , as well as on external electric fields. Electronic transport measurements allow us to deduce a value for the localization length and the density of states in our Na_2IrO_3 thin crystals devices, offering an alternative approach to study insulating layered materials.

Sodium iridate (Na_2IrO_3) and other 5d iridates have been widely studied in recent years as they have been identified as experimental realizations of the Kitaev model, an exactly solvable model that describes a set of spin-1/2 moments in a honeycomb lattice with highly anisotropic exchange interaction and exciting ground states such as spin liquids¹⁻³. In real materials such as Na_2IrO_3 , the existence of Heisenberg and off diagonal interactions benefit the appearance of magnetically ordered ground states over a spin liquid. Recent studies have explored the effect of external pressure and high magnetic fields on the ground states of Na_2IrO_3 ^{4,7,8}. First principle calculations⁴ have found that under high pressure, Na_2IrO_3 goes through successive structural and magnetic phase transitions, some of them zigzag magnetic ordered and some nonmagnetic, all with low energy excitations that can be well described by $j_{eff}=1/2$ states and in particular having some phases (with a structure corresponding to space group $P\bar{1}$)⁴ resembling a gapped spin liquid Kitaev state. Similarly, magnetic torque measurements have found that at magnetic fields up to 60T, long range spin correlations functions decay rapidly pointing to a field-induced quantum spin liquid⁸. In the absence of high pressure or magnetic fields, recent inelastic x-ray scattering measurements have reported a proximate spin liquid regime above the long-range ordering temperature, where fractional excitations are emergent, revealed by spin-spin correlations restricted to nearest neighbor sites, among other factors⁹.

Older and newer studies on Na_2IrO_3 have been limited to probes that require bulk crystals, where the insulating character of Na_2IrO_3 has hampered its integration to an electronic device, advantageous for the study and manipulation of quasiparticle excitations, of interest in topological quantum computing^{5,6}. Here we report electronic transport measurements on thin crystals of Na_2IrO_3 , where electronic transport is ruled by variable range hopping at temperatures above the magnetic ordering transition known for bulk Na_2IrO_3 (~ 15 K) and electric field assisted above a critical applied field. Fits of our data to these two mechanisms allow us to deduce the localization length as well as the density of states at the Fermi level in our Na_2IrO_3 devices. Our Angle Resolved Photoemission Spectroscopy (ARPES) measurements show a non-vanishing density of states at the Fermi level, consistent with our electronic transport experiments.

Bulk crystals of Na_2IrO_3 were grown mixing elemental Ir (99.9% purity, BASF) with Na_2CO_3 (99.9999% purity, Alfa-Aesar) in a 1 : 1.05 molar ratio. The mixture was ground for several minutes and pressed into a pellet at approximately 3,000 psi. The pellet was

subsequently warmed in a furnace to 1050 °C and held at this temperature for 48 hours, before being cooled to 900, °C over 24 hours and finally furnace-cooled. Single crystals of more than one square millimeter were collected from the surface of the pellet. Crystals were exfoliated onto a Si/SiO₂(280 nm) substrate and immediately coated with e-beam resist, minimizing the exposure to air.

Some wafers with exfoliated crystals were left uncoated and promptly analyzed through Raman spectroscopy. Raman scans were made over a range of 56 cm^{-1} to 800 cm^{-1} . Three Raman active modes were observed at 454 cm^{-1} , 484 cm^{-1} and 561 cm^{-1} (Figure 1a) consistent with the reported first-order Raman modes of bulk sodium iridate¹⁰. Exfoliated crystals were about ~ 100 nm thick, measured through atomic force microscopy (Figure 1b and c). Electrodes were patterned on the ebeam resist-coated wafers using standard electron beam lithography, previous to the deposition of Ti(4 nm)/Au(140 nm) using electron beam evaporation.

Current-voltage (IV) characteristics were measured (two probe) in a closed cycle cryostat (Oxford Instruments) from 300 K down to 1.5 K. As shown in Figure 2a, at high temperatures the IV curves show an ohmic-like behavior. As the temperature is lowered, the slope of the IV curves decreases indicating an increase of the device's resistance. At sufficient low temperatures, the IV characteristics become non-linear (Figure 2b). This behavior is consistent with the known Mott-insulating character of Na₂IrO₃. Previous numerical works that consider both Coulomb interactions and spin-orbit coupling¹¹ have been able to explain the observed insulating gap in Na₂IrO₃^{11,32} considering a Coulomb repulsion U (3eV) that is larger than the effective bandwidth (≈ 1 eV), supporting the idea of Na₂IrO₃ being a spin-orbit assisted Mott insulator.

Being an accurate measurement of the conductance of the sample at zero bias non-accessible at low temperatures, we tracked the change of the current across the sample at non-zero bias as a function of the temperature in a range of 3K-120K (see Fig. 3), and compared it to the thermal activation theory, characterized by an Arrhenius law,

$$I(T) \propto I_o e^{-E_A/k_B T} \quad (1)$$

where E_A is the activation energy and k_B is Boltzmann constant. Figure 3a shows I versus $1/k_B T$ on a semi-log plot for different bias voltages. While the data fits in small range of temperatures to a thermal activated behavior (at around 120K), it follows in a more extended

range a three-dimensional variable range hopping (VRH) mechanism¹² ($\approx 15K$ - $120K$), as shown in Figure 3b. Mott's variable range hopping (VRH) law considers 3-dimensional hopping between remote sites whose energy levels happen to be close to the Fermi level μ , as spatial neighboring sites have larger resistances¹⁸.

Typically, the hopping length increases with lowering temperature, therefore the name of variable range hopping¹⁸. In general, Mott's VRH is described by

$$I(T) \propto I_o e^{-(T_o/T)^\nu}, \quad (2)$$

with $\nu = 1/4$ for three-dimensional VRH and T_o the energy scale related to localization length of the charge carriers,

$$T_o = 21.2/k_B a^3 g_0 \quad (3)$$

with a the localization length and g_0 the density of states at the Fermi level. A fit of the data at low bias (50mV) to three-dimensional VRH yields $T_o^{1/4} = 31K^{1/4}$ (see Fig. 3b), similar to the reported values for heteroepitaxial Na_2IrO_3 thin films¹⁶.

Inspecting more carefully the data in Fig. 3b at different bias voltages, two main effects are visible. First, there is a change in the trend of the curves near $\sim 15K$ (grey line in Figures 3a and b), corresponding to the critical temperature of the long range antiferromagnetically ordered state reported for bulk crystals after magnetic susceptibility and heat capacity measurements^{13,14}, neutron and x-ray diffraction²³. The onset of long range magnetic ordering seems here to have an effect on the charge transport mechanism in the thin crystals of Na_2IrO_3 , possibly suppressing VRH below the transition temperature. A similar phenomenon has been observed in the temperature dependence of the resistivity of heteroepitaxially grown thin films of Na_2IrO_3 ¹⁶. Also, non-equilibrium optical measurements have shown signature of a long range ordered state in photoinduced reflectance measurements¹⁷. Second, as the bias voltage increases, $\ln(I)$ vs $T^{-1/4}$ deviates from a linear dependence, indicating also a divergence from a VRH mechanism.

We can understand effect 1 by taking a closer look to VRH. Following the model by Miller and Abrahams²⁴, the resistivity R_{ij} resulting from hopping over sites ij is given by:

$$R_{ij} = R_{ij}^0 \exp\left(\frac{2r_{ij}}{a} + \frac{\epsilon_{ij}}{k_B T}\right), \quad (4)$$

where r_{ij} is the spatial distance to the nearest neighboring site and ϵ_{ij} correspond to the difference of the hopping sites energies ϵ_i and ϵ_j lying in a narrow band near the Fermi

energy, whose width ϵ_o decreases with temperature and depends on the density of states at the Fermi level g_o and localization length a ,

$$\epsilon_o = \frac{(k_B T)^{3/4}}{(g_o a^3)^{1/4}} \quad (5)$$

Hopping between sites depends on both the spatial and energetic separation of the sites. If $2r_o/a \gg 1$ (with r_o the average spatial distance to the nearest neighbor empty site), the conduction mechanism is reduced to nearest neighbor hopping. If on the other hand $2r_o/a$ is of the order or less than unity, the second term in equation 4 contributes the most to the resistance and hops to sites that are further away in space but closer in energy are favored. Hopping between sites is in this case variable range, which corresponds to the transport mechanism in our thin crystals of Na_2IrO_3 above the magnetic ordering transition. In fact, Mott's VRH relation (equation 2) is derived by finding the energy ϵ_{ij} from equation 4 at which the resistivity is minimum. In the case of a magnetic ordered state, previous works have introduced an extension of Mott's VRH model in which the hopping energy ϵ_{ij} has an additional term related to the relative magnetization of the hopping sites²⁵. It is however unclear if associating a cost on the hopping energy based on the spin orientation of the hopping sites is valid, as carriers have tendency to align their spin to the localized spin^{26,27}. Based on our data, we believe that electronic transport in our Na_2IrO_3 devices in the magnetic ordered regime goes beyond Mott's VRH model.

Effect 2 caused by the bias voltage, can be unveiled by adding the effect of an electric field E to equation 4, obtaining

$$R_{ij} = R_{ij}^0 \exp \left(\frac{2r_{ij}}{a} + \frac{\epsilon_{ij} - er_{ij}E}{k_B T} \right), \quad (6)$$

At high electric field strengths, where $|er_{ij}E| \geq \epsilon_{ij}$, hopping in the direction of the electric field will compensate the difference energy between hopping sites, ϵ_{ij} . Therefore hops between sites that are closer in energy are no longer energetically favorable and the first term in equation 6 dominates. The average distance between hopping sites r is expected to satisfy $|erE| = \epsilon_{ij}$. Taking $\epsilon_{ij} \sim 1/r^3 g_o$ (where g_o is the density of states at the Fermi level) the average distance between hopping sites becomes $r \sim (1/eEg_o)^{1/4}$ giving rise to a field assisted transport mechanism²⁸

$$R_{ij} = R_{ij}^0 \exp \left(\left(\frac{E_o}{E} \right)^{1/4} \right) \quad \text{or} \quad I \propto I_o \exp \left(- \left(\frac{E_o}{E} \right)^{1/4} \right), \quad (7)$$

with E_o the characteristic localization field.

$$E_o = 1/eg_o a^4 \quad (8)$$

Above a critical external electric field, carrier hopping is therefore mediated by the electric field and there is no longer a clear VRH mechanism, as observed for the highest fields in Figure 3b. In fact, there is an electric field assisted transport at high fields that can be observed in the data, which is accentuated at lower temperatures as is shown in Figure 4, where IV curves at different temperatures are represented following relation 7. Below a critical electric field, transport is no longer field assisted. A fit of the data represented in Fig.4 to equation 7 allow us to extract E_o . In particular, for 20K we obtain $E_o^{1/4} = 190(V/m)^{1/4}$.

From the definitions of E_o (equation 8) and T_o (equation 3), we are able to deduce a localization length $a \approx 3nm$ and a density of states $g_o \approx 10^{25}/eVm^3$ in our Na_2IrO_3 thin crystal devices. Localization length is about 10 times larger than the one reported for heteroepitaxial thin films, calculated using a density of states estimated for other iridates¹⁶. Our analysis provides a value for both the localization length and the density of states in Na_2IrO_3 thin crystals deduced from the same set of data.

Mott's VRH requires a non-vanishing density of states at the Fermi level, as hopping between sites are concentrated in a band near the Fermi energy with a bandwidth ϵ_o (eqn. 5). Our ARPES measurements confirm this in our samples.

ARPES measurements were performed at Beamline 4.0.3 (MERLIN) at the advanced light source using 90 eV photons. Vacuum was better than 5×10^{-11} Torr. The total energy resolution was 20 meV with angular resolution ($\Delta\theta \leq 0.2^\circ$). Data was taken at 290K to avoid charging of the sample. A fresh crystal of Na_2IrO_3 (as those used for the electronic device fabrication) was mounted and cleaved in-situ the ARPES chamber. Figure 5a shows the measured electronic band structure along the high symmetry direction Γ -M with a photon energy of 90eV. A feature near the Fermi energy is visible, as reported in previous ARPES works. Initially, this in-gap feature was identified as a metallic surface state³⁰ but later on it was found through spatially resolved-ARPES measurements³¹ that it was consequence of quasiparticle formation in one of the possible cleavage planes of Na_2IrO_3 . Indeed, the edge sharing IrO_6 octahedra in Na_2IrO_3 form a layered stacking alternating with pure Na layers, which gives rise to both Na and Ir-O terminated surfaces after cleavage. In the former, the Ir-O octahedra being embedded between two Na layers, create a charge transfer from Na to

Ir giving rise to a quasiparticle at the Fermi level³¹. This band formed at one of the possible terminations in Na_2IrO_3 after cleavage (the Na-terminated) is what we believe mediates the VRH mechanism in our Na_2IrO_3 devices. In the frame of Mott's VRH, the width of the band responsible for conduction (eqn. 5) at 290K, corresponding to the ARPES measurements, is $\approx 90\text{meV}$, which falls within the quasiparticle observed in Fig. 5. Fig. 5b shows energy distribution curves (EDC) in correspondance of the quasiparticle (in black, at Γ) and at a larger momentum outside (in red) that testifies a non-vanishing density of states at the Fermi level, as required by Mott's VRH.

After cleavage, the Na and O terminated surfaces are approximately $10\text{-}40\ \mu\text{m}$ large, as demonstrated through μARPES ³¹. Our ARPES data being taken with a spotsize of $\approx 100\mu\text{m}$, captures an average of the two terminations. However, the spectral weight measured in the vicinity of the Fermi level is to be attributed to the Na-terminated surface only, since the Ir-O surface has no states in that energy range³¹. This does not invalidate any of our conclusions and in fact supports them, since this density of states is also representative of the bulk, which we probe with our transport measurements. The band structure characteristic of the Ir-O cleave that lacks of states near the Fermi energy, is instead an "anomaly" given the absence of the Na layer which causes a difference charge balance between the two topmost layers of the cleave³¹. Therefore, the electronic structure as measured by ARPES, both here and in refs. 30 and 31, does show a small density of states within a small range from the Fermi level.

In conclusion, we have integrated a thin crystal of Na_2IrO_3 into an electronic device, presenting the same Raman active modes as for the bulk crystals. We have observed that the main transport mechanism at temperatures above the formation of an antiferromagnetic long range order ($\approx 15\text{K}$) is VRH. This observation is supported by ARPES measurements at the high temperature end (290K) that testify a non-vanishing density of states at the Fermi level as required by Mott's VRH. We have observed that as the system approaches long range order, it deviates from VRH with no evidence of this mechanism below the ordering temperature. Similarly, we have found that in the presence of an external electric field, transport diverges from VRH, becoming field assisted. Contrasting our data to the Mott's VRH and electric field assisted models allow us to deduce a localization length of $\approx 3\text{nm}$ and a density of states of $\approx 10^{25}/\text{eVm}^3$ in our Na_2IrO_3 thin crystal devices. Our work constitutes a first approach to integrate an exfoliated thin crystal of Na_2IrO_3 into an electronic device,

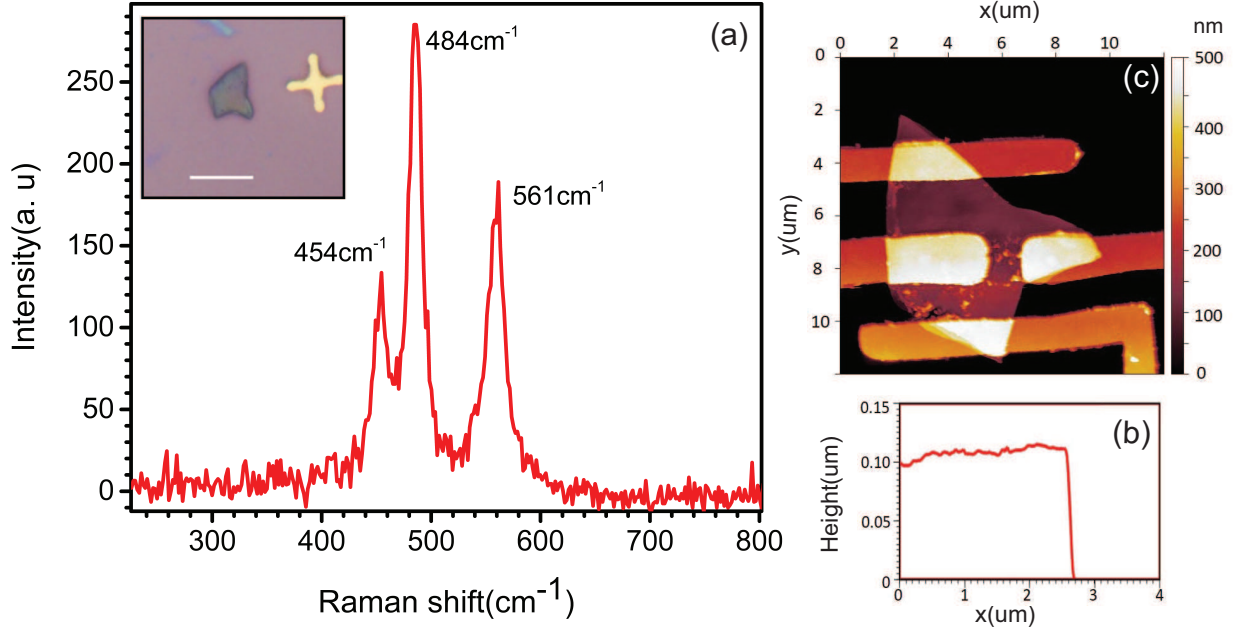


FIG. 1. **(a)** Raman spectra of an exfoliated thin crystal of Na_2IrO_3 . Inset: Optical image of the crystal used for device fabrication (scale bar $10\ \mu\text{m}$). **(b)** Atomic force microscopy scan of the electronic device. Electrodes used for the two probe measurements were middle left and bottom. **(c)** AFM height profile of the device, crystal is approximately $100\ \text{nm}$ thick.

where separate ARPES measurements inform the electronic transport experiments. Using these two experimental techniques independently on similarly prepared samples can unveil important properties in other layered materials.

ACKNOWLEDGMENTS

The primary funding for this work was provided by the U.S. Department of Energy, Office of Science, Office of Basic Energy Sciences under contract DE-SC0018154. The Advanced Light Source is supported by the Director, Office of Science, Office of Basic Energy Sciences, of the U.S. Department of Energy (U.S. DOE-BES) under contract no. DE-AC02-05CH11231. Work by J.G.A., G.L., V.N. and N.P.B. was supported by the Department of Energy *Early Career Program*, Office of Basic Energy Sciences, Materials Sciences and Engineering Division, under Contract No. DE-AC02-05CH11231 for crystal growth. P. S

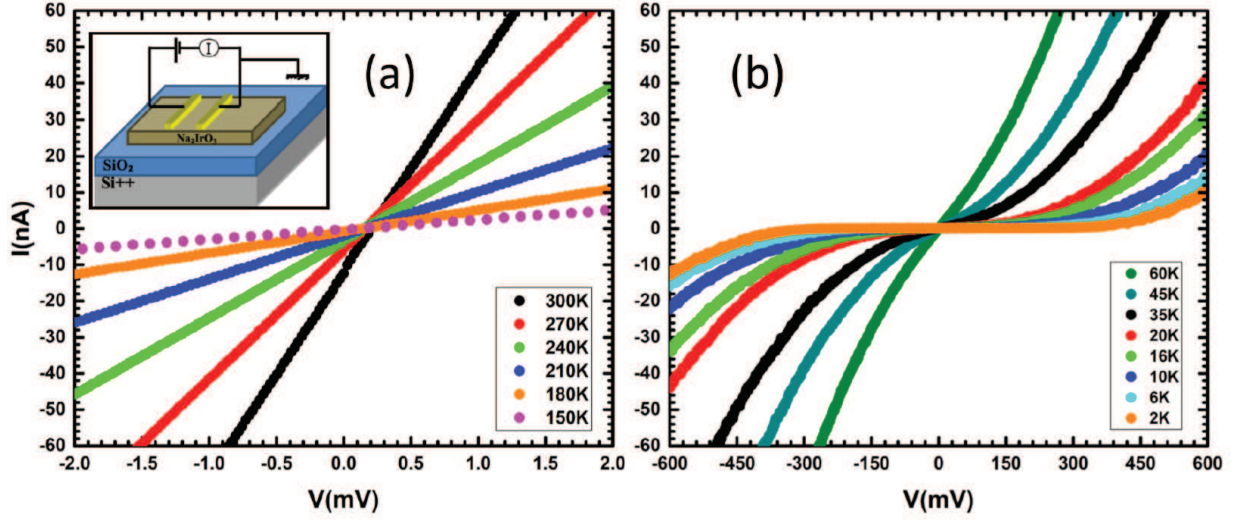


FIG. 2. (a) IV characteristics of the Na_2IrO_3 device at high temperatures. Inset: schematics of the electronic device. (b) Non-linear IV curves at low temperatures down to 2 K.

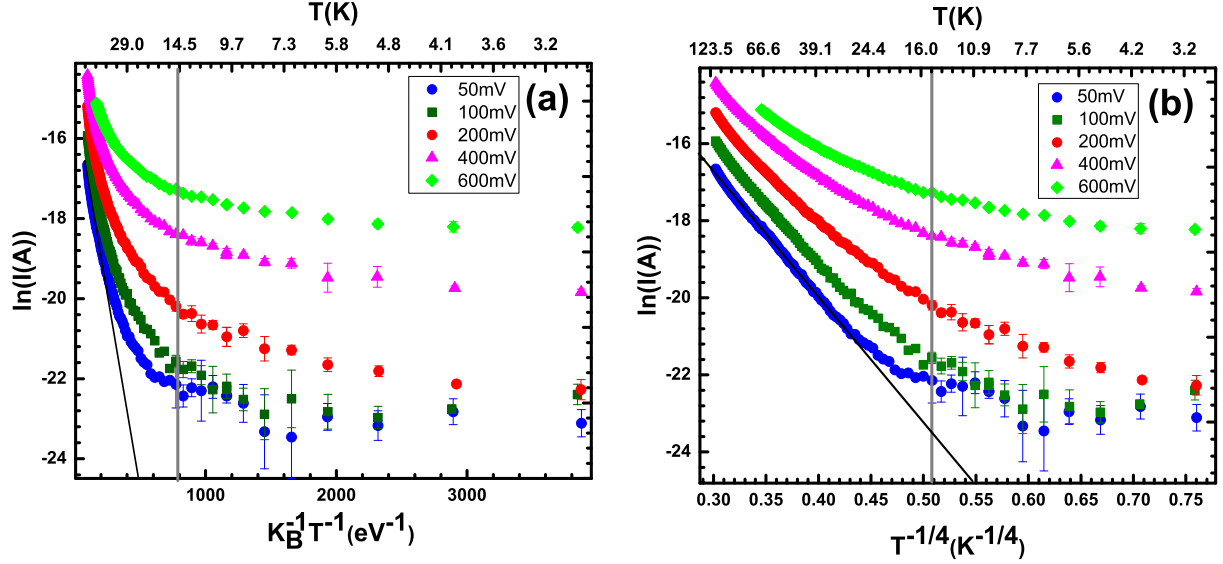


FIG. 3. Temperature dependence of the current I at different bias voltages 50 mV, 200 mV, 400 mV and 600 mV, extracted from the measured IV characteristics. Temperature range is 3K - 120K (a) I versus $1/k_B T$ and (b) I versus $T^{-1/4}$ on a semi-log plot.

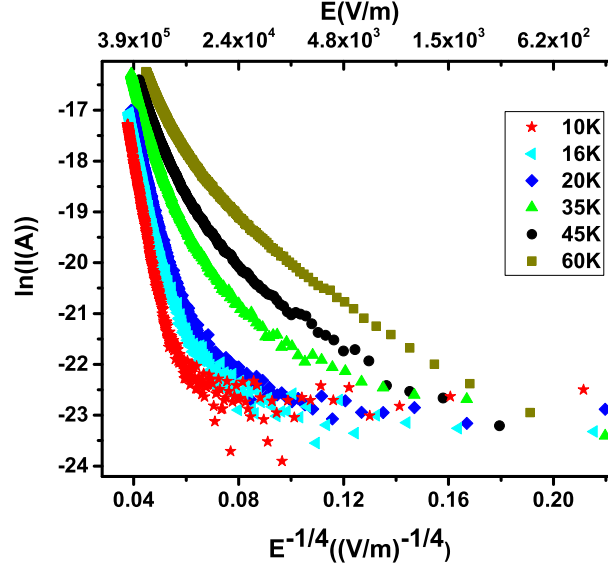


FIG. 4. Electric field dependence of the current I versus $E^{-1/4}$ in a temperature range 10K-60K

and H. T. were supported by the National Institute of General Medical Sciences of the National Institutes of Health under Award Numbers UL1GM118979, TL4GM118980, and RL5GM118978 for Raman measurements. The content is solely the responsibility of the authors and does not necessarily represent the official views of the National Institutes of Health. We would like to acknowledge Luca Moreschini for valuable advice on the ARPES data as well as Jonathan Denlinger for assistance during the ARPES experiments.

REFERENCES

- ¹Sae Hwan Chun, Jong-Woo Kim, Jungho Kim, H. Zheng, Constantinos C. Stoumpos, C. D. Malliakas, J. F. Mitchell, Kavita Mehlawat, Yogesh Singh, Y. Choi, T. Gog, A. Al-Zein, M. Moretti Sala, M. Krisch, J. Chaloupka, G. Jackeli, G. Khaliullin and B. J. Kim, Nat. Phys. **11**, 462 (2015).
- ²Yogesh Singh, S. Manni, J. Reuther, T. Berlijn, R. Thomale, W. Ku, S. Trebst, and P. Gegenwart, Phys. Rev. Lett. **108**, 127203 (2012).
- ³Stephen M Winter, Alexander A Tsirlin, Maria Daghofer, Jeroen van den Brink, Yogesh Singh, Philipp Gegenwart and Roser Valent, J. Phys.: Condens. Matter **29**, 493002 (2017).
- ⁴Kaige Hu, Zhimou Zhou, Yi-Wen Wei, Chao-Kai Li, and Ji Feng, Phys. Rev. B **98**, 100103(R) (2018).

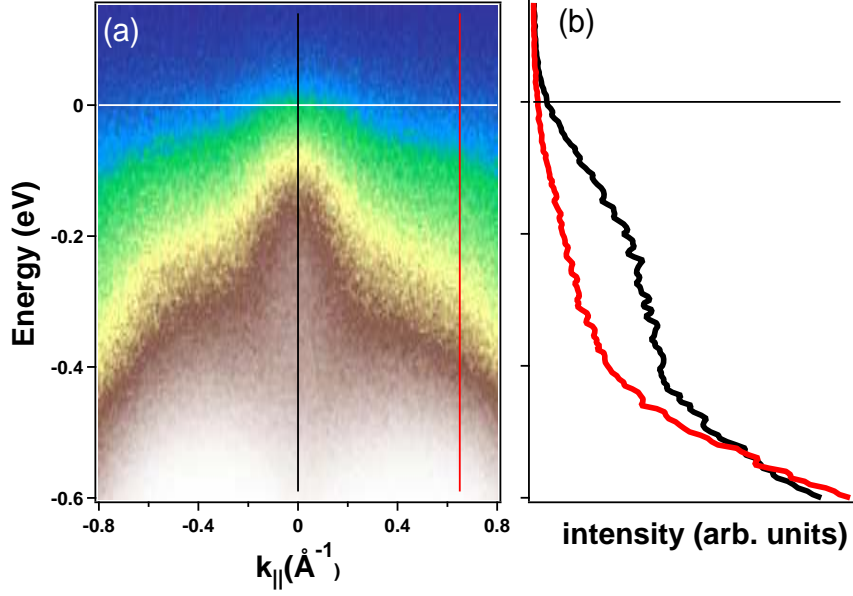


FIG. 5. (a) Measured electronic band structure along the high symmetry direction Γ -M with photon energy 90 eV (b) Energy distribution curves integrated over 0.04\AA^{-1} around Γ (black) and at 0.65\AA^{-1} as indicated in (a) by the red and black lines.

⁵Alexei Kitaev Annals of Physics **321**, 2 (2006).

⁶Y. Kasahara, T. Ohnishi, Y. Mizukami, O. Tanaka, Sixiao Ma, K. Sugii, N. Kurita, H. Tanaka, J. Nasu, Y. Motome, T. Shibauchi and Y. Matsuda, Nature **559**, 227 (2018).

⁷Xiaoxiang Xi, Xiangyan Bo, X. S. Xu, P. P. Kong, Z. Liu, X. G. Hong, C. Q. Jin, G. Cao, Xiangang Wan and G. L. Carr Phys. Rev. B **98**, 125117 (2018).

⁸Sitikantha D. Das, Sarbajaya Kundu, Zengwei Zhu, Eundeok Mun, Ross D. McDonald, Gang Li, Luis Balicas, Alix McCollam, Gang Cao, Jeffrey G. Rau, Hae-Young Kee, Vikram Tripathi, and Suchitra E. Sebastian, Phys. Rev. B **99**, 081101(R) (2019).

⁹A. Revelli, M. Moretti Sala, G. Monaco, C. Hickey, P. Becker, F. Freund, A. Jesche, P. Gegenwart, T. Eschmann, F. L. Buessen, S. Trebst, P. H. M. van Loosdrecht, J. van den Brink and M. Gruninger, ArXiv: 1905.13590

¹⁰Satyendra Nath Gupta, P. V. Sriluckshmy, Kavita Mehlawat, Ashiwini Balodhi, Dileep K. Mishra, S. R. Hassan, T. V. Ramakrishnan, D. V. S. Muthu, Yogesh Singh and A. K. Sood EPL **114**, 47004 (2016).

¹¹R. Comin, G. Levy, B. Ludbrook, Z.-H. Zhu, C. N. Veenstra, J. A. Rosen, Yogesh Singh, P. Gegenwart, D. Stricker, J. N. Hancock, D. van der Marel, I. S. Elfimov and A. Damascelli,

- Phys. Rev. Lett. **109**, 266406 (2012).
- ¹²N. F. Mott, Phil. Mag. **8**, 835 (2006).
- ¹³Yogesh Singh and P. Gegenwart, Phys. Rev. B **82**, 064412 (2010).
- ¹⁴X. Liu, T. Berlijn, W.-G. Yin, W. Ku, A. Tsvelik, Young-June Kim, H. Gretarsson, Yogesh Singh, P. Gegenwart and J. P. Hill, Phys. Rev. B **83**, 220403R (2011).
- ¹⁵Feng Ye, Songxue Chi, Huibo Cao, Bryan C. Chakoumakos, Jaime A. Fernandez-Baca, Radu Custelcean, T. F. Qi, O. B. Korneta, and G. Cao, Phys. Rev. B **85**, 180403R (2012).
- ¹⁶Marcus Jenderka, Jos Barzola-Quiquia, Zhipeng Zhang, Heiko Frenzel, Marius Grundmann and Michael Lorenz, Phys. Rev. B **88**, 045111 (2013).
- ¹⁷J. P. Hinton, Patankar, E. Thewalt, A. Ruiz, G. Lopez, N. Breznay, A. Vishwanath, J. Analytis, J. Orenstein, J. D. Koralek and I. Kimchi, Phys. Rev. B **92**, 115154 (2015).
- ¹⁸B.I. Shklovskii and A.L. Efros, "Electronic Properties of Doped Semiconductors" (Springer-Verlag, Berlin Heidelberg, 1984) Chap. 9, pp. 202-210.
- ¹⁹B.I. Shklovskii and A.L. Efros, "Electronic Properties of Doped Semiconductors" (Springer-Verlag, Berlin Heidelberg, 1984) Chap. 10, pp. 228-238.
- ²⁰V.Yu. Butko, J. F. DiTusa, and P.W. Adams, Phys. Rev. B **84**, 1543 (2000).
- ²¹A. L. Efros and B. I. Shklovskii, J. Phys. C: Solid State Phys. **8**, L49 (1975).
- ²²S. K. Choi, R. Coldea, A. N. Kolmogorov, T. Lancaster, I. I. Mazin, S. J. Blundell, P. G. Radaelli, Y. Singh, P. Gegenwart, K. R. Choi, S.-W. Cheong, P. J. Baker, C. Stock, and J. Taylor, Phys. Rev. Lett. **108**, 127204 (2012).
- ²³F. Ye, S. Chi, H. Cao, B. C. Chakoumakos, J. A. Fernandez-Baca, R. Custelcean, T. F. Qi, O. B. Korneta, and G. Cao, Phys. Rev. B **85**, 180403 (2012).
- ²⁴B.I. Shklovskii and A.L. Efros, "Electronic Properties of Doped Semiconductors" (Springer-Verlag, Berlin Heidelberg, 1984) Chap. 4, pp. 74-93.
- ²⁵P. Wagner, I. Gordon, L. Trappeniers, J. Vanacken, F. Herlach, V. V. Moshchalkov, and Y. Bruynseraede, Phys. Rev. B **81**, 3980 (1998).
- ²⁶Sudhakar Yarlagadda, Phys. Rev. Lett. **84** 4017 (2000).
- ²⁷P.G. de Gennes, Phys. Rev. **118**, 141 (1960).
- ²⁸B.I Shklovskii, Sov. Phys. Semicond. **6**, 1964-1967 (1973).
- ²⁹S. Chikara, O. Korneta, W. P. Crummett, L. E. DeLong, P. Schlottmann and G. Cao, J. Appl. Phys. **107** 09D910 (2010).
- ³⁰Nasser Alidoust, Chang Liu, Su-Yang Xu, Ilya Belopolski, Tongfei Qi, Minggang Zeng,

- Daniel S. Sanchez, Hao Zheng, Guang Bian, Madhab Neupane, Yu-Tzu Liu, Stephen D. Wilson, Hsin Lin, Arun Bansil, Gang Cao, and M. Zahid Hasan, Phys. Rev. B **93**, 245132 (2016).
- ³¹L. Moreschini, I. Lo Vecchio, N. P. Breznay, S. Moser, S. Ulstrup, R. Koch, J. Wirjo, C. Jozwiak, K. S. Kim, E. Rotenberg, A. Bostwick, J. G. Analytis, and A. Lanzara Phys. Rev. B **96**, 161116(R) (2017).
- ³²C. H. Sohn, H.-S. Kim, T. F. Qi, D. W. Jeong, H. J. Park, H. K. Yoo, H. H. Kim, J.-Y. Kim, T. D. Kang, Deok-Yong Cho, G. Cao, J. Yu, S. J. Moon and T. W. Noh, Phys. Rev. B **88**, 085125 (2013).